High-temperature structure of Co_3O_4: Understanding spinel inversion using *in situ* and *ex situ* measurements

Taylor D. Sparks*
Department of Materials Science and Engineering, University of Utah, Salt Lake City, Utah 84112, USA

Aleksander Gurlo
Institute for Material Science and Technologies, Technische Universität Berlin, D-10587 Berlin, Germany

Maged F. Bekheet
Fachgebiet Keramische Werkstoffe, Institut für Werkstoffwissenschaften und -technologien, Technische Universität Berlin, Hardenbergstraße 40, 10623 Berlin, Germany

Michael W. Gaultois
Leverhulme Research Centre for Functional Materials Design, The Materials Innovation Factory, Department of Chemistry, University of Liverpool, 51 Oxford Street, Liverpool L7 3NY, United Kingdom

Gennady Cherkashinin
Fachbereich Material- und Geowissenschaften Fachgebiet Oberflächenforschung, Technische Universität Darmstadt, Darmstadt 64287, Germany

Laetitia Laversenne
Université Grenoble Alpes, CNRS, Grenoble INP, Institut Néel, 38000 Grenoble, France

David R. Clarke
School of Engineering and Applied Sciences, Harvard University, Cambridge, Massachusetts 02138, USA

(Received 5 June 2018; published 13 March 2019)

In this paper we investigate the high-temperature structure of Co_3O_4, a compound that has been studied extensively over the last 60 years due to its unresolved high-temperature structure. *In situ* thermal analysis and x-ray diffraction confirm previously reported high-temperature structural changes and show that these changes are unrelated to the high-temperature decomposition to CoO. Raman-active peaks are also extinguished over the same temperature range. By considering the changing lattice parameter, *A*-O, and *B*-O bond lengths as well as cation size we are able to calculate the degree of inversion which reaches a maximum of 0.6. To further study the structure in this experimentally inaccessible range we quench samples and perform *ex situ* measurements including redox titration, x-ray photoelectron spectroscopy, and neutron diffraction. We do not observe any evidence of large oxygen vacancy concentrations or octahedral Co_B^{3+} ions with high spin state. However, we do show an evolution in the magnetic moment from magnetic structure refinement from (2.4 μ_B) to (2.7 μ_B) that coincides exactly with the high-temperature anomaly and suggests partial inversion (0.46) of the spinel structure in fairly good agreement with the inversion calculated from bond lengths.

DOI: 10.1103/PhysRevB.99.104104

I. INTRODUCTION

Cobalt oxide spinel, Co_3O_4, is a well-known antiferromagnetic oxide investigated most recently as a promising catalyst for oxygen evolution reactions in artificial photosynthesis [1,2]. The compound crystallizes in the spinel crystal structure featuring twice as many six-coordinate (octahedral) cation sites as four-coordinate (tetrahedral) sites. In order to maintain charge neutrality with the oxygen anions, there must be two Co^{3+} ions and one Co^{2+} ion per formula unit.

How the two different ions arrange themselves over the tetrahedral cation sites (often called the *A* site) or octahedral cation sites (often called the *B* site) dictates many important electrical and magnetic properties in spinels. The low-temperature structure of Co_3O_4 is considered the archetypal *normal* spinel because the Co^{2+} ions completely occupy the tetrahedral *A* site and Co^{3+} ions completely occupy the octahedral *B* site. Neutron diffraction and magnetic susceptibility measurements suggest the d^6 electrons from Co^{3+} pair up to completely fill the octahedral t_{2g} triplet, whereas the d^7 electrons from Co^{2+} on the tetrahedral site leave three unpaired electrons on t_2 orbitals that account for the observed magnetic moment of 2.6 μ_B to 3.25 μ_B [3–5].

*sparks@eng.utah.edu

In contrast, the details of the high-temperature crystal structure of Co_3O_4 are not well understood and have been an active area of research. A variety of observations including a sudden nonlinear increase in lattice parameter [6–8], excess thermal expansion [9], electromotive force measurements on the oxygen partial pressure [7,10], opposite changes in the *A*-O and *B*-O bond lengths with increasing temperature [8], electrical conductivity and thermopower [9,11], and a phase transformation from heat capacity measurements [12], all indicate a high-temperature structural anomaly.

The exact origin of the high-temperature structural anomaly is obfuscated by two potential mechanisms as well as the incipient decomposition to rocksalt-type CoO (1165–1270 K) [7]. One mechanism is cation antisite disorder, termed *inversion* of the spinel structure, where Co^{3+} ions sit on the tetrahedral *A* site and Co^{2+} ions on the octahedral *B* site. The other mechanism is a low-spin (LS) to high-spin (HS) spin state transition of Co^{3+} ions on the octahedral sites between 1000 and 1200 K that has been suggested by many researchers [7,8,10,12]. There is currently no consensus on how much, if any, cation antisite disorder is present. Chen [13] summarizes that some authors suggest a complete inversion of the structure [7] (i.e., $Co_A{}^{3+}$ and $Co_B{}^{2+}Co_B{}^{3+}$), while others favor complete antisite disorder [8], and still others propose a retention of the normal spinel structure with only 5%–10% disorder [12].

High-temperature *in situ* magnetic susceptibility, x-ray photoelectron spectroscopy (XPS), and neutron-diffraction measurements to settle the ambiguity are hampered by the low Néel temperature ≈40 K of Co_3O_4 and lack of high-temperature instrumentation. Nevertheless, there are several *in situ* techniques remaining to study the high-temperature structure of Co_3O_4 including Raman spectroscopy and thermogravimetric analysis (TGA) discussed in this work, and thermopower which will be discussed in detail in a subsequent contribution [14]. Furthermore, in this contribution we attempt to preserve the high-temperature structure via quenching and then use *ex situ* XPS, neutron diffraction, and redox titration measurements on the samples to gain additional insight. Finally, *in situ* phase composition is monitored via spectroscopy and diffraction to ensure that the high-temperature anomaly is unrelated to the transformation from Co_3O_4 to CoO.

II. EXPERIMENT

Disk-shaped pellets were fabricated from nanometer-sized Co_3O_4 powder (Sigma Aldrich, 99.9 wt %, 50-nm particles). The powders were first cold-pressed with a 6-ton load in a $\frac{1}{2}$-in. die and then sintered in air. Pure phase, dense samples of Co_3O_4 and CoO were obtained by firing the samples from room temperature up to 1148 K over 2 h and holding for 6 h, ramping to 1373 K over 1 h and holding for 6 h, ramping back to 1148 K over 2 h and holding for 2 h. From this point, samples were quenched in air to obtain phase-pure CoO, or slowly cooled at 1 K/min to obtain phase-pure Co_3O_4. Intermediate cooling rates resulted in mixtures of CoO and Co_3O_4 phases. *Ex situ* magnetic structure determination, XPS, and redox titration measurements were performed on samples that were quenched from high temperature by submersion in liquid nitrogen.

Property measurement

X-ray diffraction from room temperature up to 1273 K was performed in air using a PANalaytical X'Pert Pro diffractometer in continuous-scanning mode at 40 kV 45 mA with a vertical θ-θ scanning geometry from 20° to 100° with a step size of 0.017° and a rate of 1.40 s/step. The height of the sample in the furnace was zeroed by breaking the beam and tilt was corrected by rocking the sample. Iron-filtered Co $K\alpha$ radiation was used, except for the room temperature x-ray diffraction (XRD) of CoO quenched and intermediate cooled samples, where nickel-filtered Cu $K\alpha$ radiation was used. Measurements at temperature were made with an Anton-Paar HTK1200N furnace to heat the samples for high-temperature data collection. The temperature fluctuation within the furnace was less than 1 K, and the sample was heated slowly at 5 K/min and allowed to equilibrate 30 min before each scan was performed. Measurements were performed at 300, 800, 875, 950, 1025, 1100, 1140, 1163, and 1273 K, and an additional measurement was made after cooling back to 300 K.

Raman spectra were obtained as a function of temperature in air using a confocal LabRAM ARAMIS Raman Microscope (HORIBA Scientific) with the sample in a Linkam heating stage (Scientific Instruments Ltd., Waterford Surrey, England). The spectra were excited with a 515-nm laser (Kimmon Electric US, Ltd. IK Series He-Cd LASER Englewood, CO, USA). Spectra were recorded from room temperature (298 K) up to a temperature of 1223 K and back down to room temperature and with a constant heating and cooling rate (10 K/min). Spectral analysis such as baseline adjustment, smoothing, and normalization, was performed using GRAMS software package (Galactic Industries Corporation, Salem, NH, USA).

Neutron-diffraction measurements were performed on the two-axis diffractometer D1B at the Institut Laue Langevin (ILL, Grenoble, France). Powdered sample was loaded into a vanadium can and placed in a cryostat; diffractograms were recorded with a wavelength of $\lambda = 2.52$ Å.

Nuclear structure determination and refinement was performed using the full-pattern Rietveld method based on least-squares refinement in the GSAS and EXPGUI software packages [15,16]. Magnetic structure determination was performed with the full-pattern Rietveld method using the FULLPROF and BASIREPS software packages [17,18]. The magnetic structure was refined based on the known structure previously determined by Roth [4]. Heat-capacity measurements performed elsewhere exhibit a sharp, lambda-type anomaly at the Néel temperature [19,20], suggesting the transition is strongly second order. Accordingly, the space group above the ordering temperature was used for refinement of the magnetic structure.

Thermogravimetry–differential thermal analysis characterization was performed on TGA Q5000 (TA Instruments, New Castle, DE, USA) on powdered samples in dynamic conditions (synthetic air or Ar, 10 ml/min) with a heating and cooling rate of 10 K/min.

Finely ground powders of Co_3O_4 annealed and quenched from 300, 773, and 1173 K were pressed into indium foil, mounted on an electrically grounded sample holder, and analyzed with a chamber base pressure of $\sim 10^{-9}$ mbar. XPS spectra were collected using a PHI 5000 VersaProbe spectrometer and a monochromatic Al $K\alpha$ (1486.7 eV) x-ray source; the diameter of the analysis area was $\sim 100\,\mu$m, and the electron escape angle was fixed at 45°. High-resolution photoelectron spectra of the Co 2*p*, Co 3*s*, O 1*s*, and C 1*s* core levels were collected using a pass energy of 11.75 eV and a step size of 0.05 eV. At this pass energy, the resolution is less than 0.6 eV, determined by analysis of the Ag $3d_{5/2}$ FWHM of a clean Ag foil; the precision of the measured binding energies (BE) is better than ±0.10 eV. A dual-beam charge neutralizer was used to prevent surface charging during measurements; the system is equipped with a low-voltage electron gun and a floating ion gun generating a low-energy ion beam. All spectra were calibrated using the C 1*s* core line arising from adventitious carbon with a fixed value of 284.8 eV, and a Shirley-type function was applied to remove the background arising from electron energy loss.

The mean oxidation state of cobalt was determined by the redox titration method adapted from Gayduk and Pantaler [21]. In a typical analysis, the powdered sample (9 mg) was dissolved in 100 ml hydrochloric acid solution (6 N) mixed with 35 ml of indigo carmine solution (0.004 N). The resulted solution was cooled to room temperature and the excess of indigo carmine was titrated by potassium bromate (0.001 N).

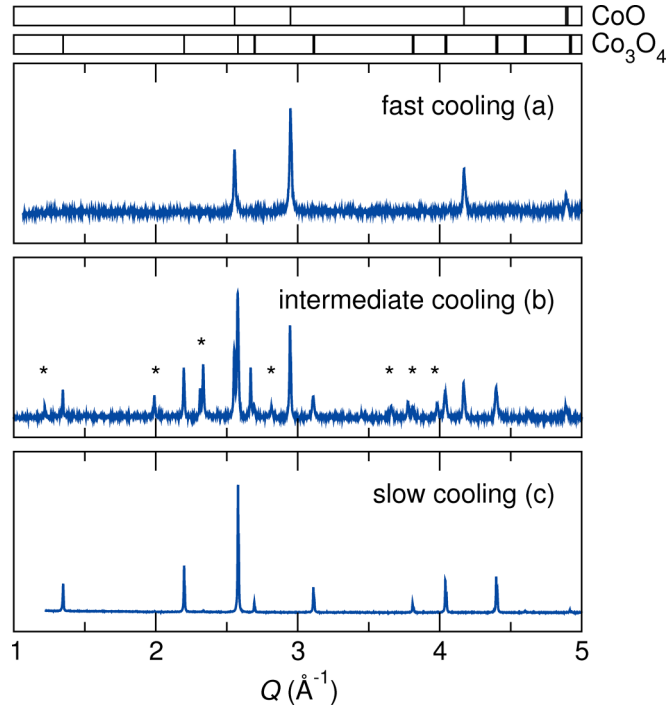

FIG. 1. X-ray diffraction patterns for (a) single-phase CoO obtained by fast cooling, (b) mixed phase Co_3O_4 and CoO samples obtained by intermediate cooling rates, and (c) single-phase Co_3O_4 obtained by slow cooling. The poor signal-to-noise ratio for CoO is due to fluorescence from using Cu $K\alpha$ radiation. Asterisks denote peaks arising from the Al_2O_3 crucible used for the reaction.

III. RESULTS AND DISCUSSION

According to the calculated binary Co-O phase diagrams [22,23], Co_3O_4 decomposes at elevated temperatures to CoO, and then to Co. The region of Co_3O_4 stability depends strongly on oxygen partial pressure as well as the size of Co_3O_4 crystallites and their surface hydroxylation, shifting to higher temperatures with decreasing crystallite size and increasing oxygen partial pressure. For example, bulk Co_3O_4 decomposes to CoO at 1242 K when $p(O_2) = 1$ bar, while it decomposes at 909 K when $p(O_2) = 10^{-6}$ bar [22,23]. There are two studies that report significantly lower temperatures. Results of *in situ* heating infrared emission spectroscopy have indicated the disorder of the spinel Co_3O_4 begins at 873 K and conversion to the rocksalt CoO occurs at 923 K [24]. There is also a high-temperature x-ray diffraction study that reports the transformation of Co_3O_4 to a disordered spinel occurs at 1150 K [8].

Our initial attempts to produce a dense sample of Co_3O_4 by sintering resulted in a mixture of spinel Co_3O_4 and rocksalt CoO. Accordingly, we varied the sintering conditions and heating/cooling rates to determine the optimum conditions for producing phase-pure Co_3O_4. Through repeated trials, we found that dense samples of phase-pure spinel Co_3O_4 could be reproducibly prepared by sintering at 1148 K and then slowly cooling at 1 K/min. CoO was produced if the samples were quenched from 1148 K instead of cooling slowly. These results are summarized in Fig. 1.

Additional information concerning the phase stability of spinel Co_3O_4 was obtained by Raman spectroscopy, thermal analysis, and high-temperature XRD. Figure 2 shows the Raman spectroscopy results of samples heated from room temperature to 1200 K and then cooled. At room temperature five Raman peaks are observed corresponding to the F_{2g}, E_g, and A_{1g} Raman-active phonon modes reported by Hadjiev *et al.* for Co_3O_4 [25]. With increasing temperature these peaks broaden, shift to lower wave numbers, and decrease in intensity. Rocksalt CoO has no Raman-active modes and none are observed at the highest temperatures. However, the Raman modes for Co_3O_4 are unexpectedly extinguished in the same temperature regime, 600–1000 K, where other high-temperature anomalies are observed. Upon cooling, the CoO to Co_3O_4 reaction is reversible and the same behavior is observed.

A more probable reason for the Raman mode extinction is locally changing the temperature at the spot illuminated by Raman laser. This suggestion is supported by previous studies on cobalt and iron oxide demonstrating that even low-power laser pulses can cause enough local heating sufficient to meaningfully alter Raman spectra and oxidation states [26,27]. On the other hand, possible effects such as photoluminescence, which is superposed with the Raman modes as temperature increases or inversion of the spinel structure, cannot be completely ruled out. One notes the inversion implies that Co^{2+} ions will increasingly occupy the *B* site in the spinel structure yielding an octahedral arrangement similar to rocksalt making them dominant in the vibration properties of Co_3O_4 and thereby removing Raman-active modes. However,

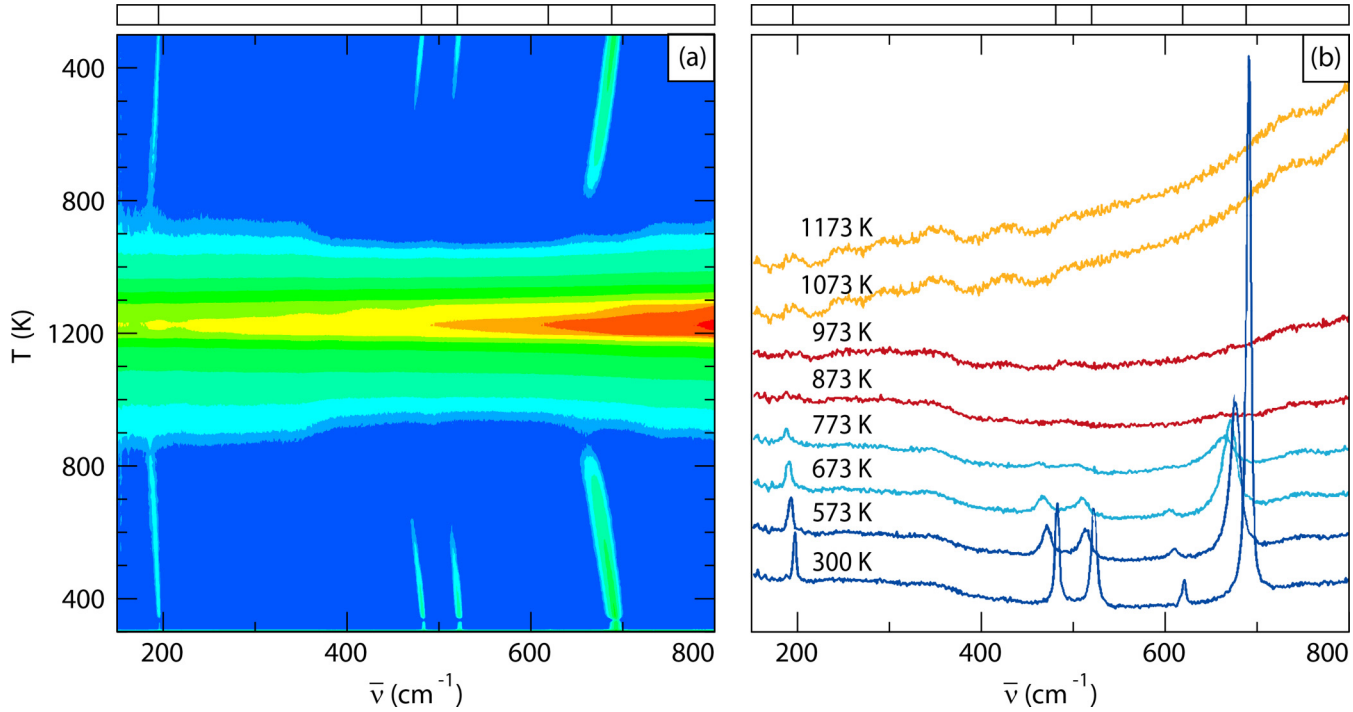

FIG. 2. (a) *In situ* Raman spectroscopy of samples heated from room temperature up to 1200 K and then cooled again. (b) Peaks corresponding to Co_3O_4 are observed but are extinguished between 600 and 1000 K, long before the transformation to CoO that begins at 1165 K (determined by TGA).

further investigations are needed to specify the dominating effect.

The thermal analysis data shown in Fig. 3 indicates that Co_3O_4 decomposition in air starts at ∼1165 K and is completed by ∼1270 K. The observed weight loss of 6.4% corresponds well to the theoretical weight loss of 6.6% for the decomposition: $Co_3O_4 \rightarrow 3CoO + \frac{1}{2}O_2$.

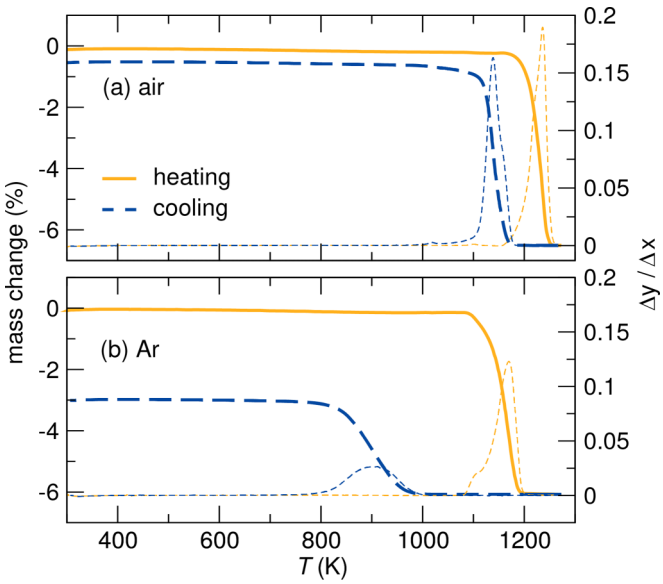

FIG. 3. Thermogravimetric analysis and differential thermal analysis of Co_3O_4 samples in air (a) and Ar (b). The sample transforms to CoO at 1165 K in air and 1084 K in Ar. In both cases, the weight loss corresponds to that expected by the loss of oxygen in Co_3O_4. Unexpectedly, the sample in Ar regains a portion of the lost weight, likely due to reaction with residual oxygen in the instrument chamber.

Upon slow cooling (10 K/min) in air, the increase in the specimen weight is observed at $T < 1100$ K, owing to the reoxidation of CoO to Co_3O_4. The reoxidized specimen nearly reaches its initial weight; the small weight difference of about 0.5% corresponds to $x = 0.08$ in Co_3O_{4-x}, implying a nearly stoichiometric composition with a minimal concentration of oxygen vacancies.

In an argon atmosphere, the Co_3O_4 decomposition starts at a lower temperature (∼1084 K) and is completed by ∼1200 K with the same weight loss. Upon slow cooling, the increase in the specimen weight is observed at $T < 990$ K, likely owing to incomplete oxidation of CoO to Co_3O_4 by residual oxygen in the instrument.

Quenching samples is performed to preserve the high-temperature electronic and crystal structure. However, given that inversion is accomplished by the transfer of an electron, and electron dynamics are generally associated with picosecond timescales, quenching in liquid nitrogen is likely insufficiently quick to preserve any possible electron transfer that is present only at high temperature. Nevertheless, neutron diffraction and XPS and redox titration results both provide evidence of a systematic electronic/magnetic/crystal structure transition as a function of quenching temperature. This systematic change in the quenched samples could be due to oxygen vacancies. However, as with TGA, redox titration (see Fig. 4) indicates a negligible concentration of oxygen vacancies below 1100 K.

The results of the *in situ* XRD characterization agree with the results of the thermal analysis. According to analysis of

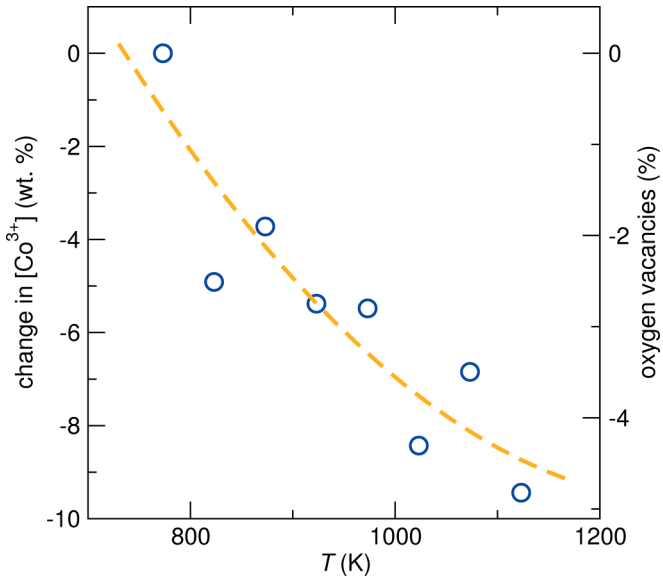

FIG. 4. Redox titration analysis of Co^{3+} reveals a small amount of oxygen vacancies, which increases with quenching temperature of Co_3O_4.

the x-ray-diffraction patterns, the spinel Co_3O_4 remains phase pure from room temperature up to 1163 K upon heating in air (Fig. 5). By 1273 K, Co_3O_4 had completely decomposed to the rocksalt structured CoO (see Table I and Fig. 5). This decomposition was reversible: upon cooling in air the CoO oxidized back to phase-pure spinel Co_3O_4. Specimens quenched to retain the rocksalt CoO phase remain stable in air on heating from room temperature until 950–1188 K, where they are oxidized to Co_3O_4. As the temperature is increased

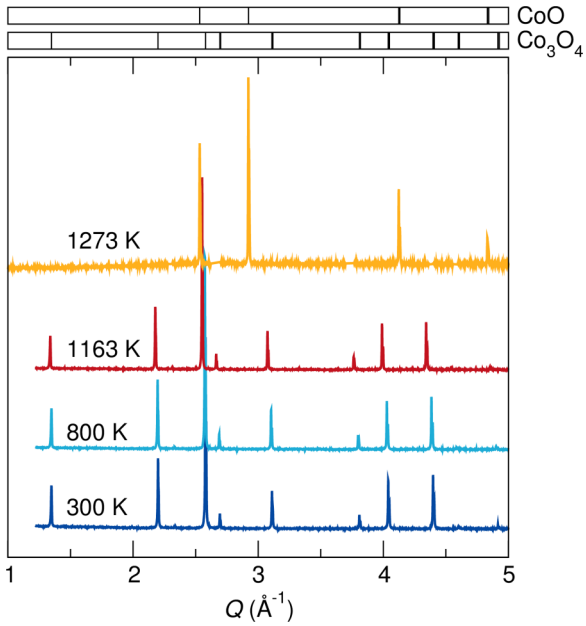

FIG. 5. *In situ* x-ray diffraction of Co_3O_4 on heating from room temperature to 1273 K. The sample converts entirely to CoO between 1163 and 1273 K.

further, above 1188 K Co_3O_4 again decomposes reversibly to 100 wt % CoO.

The results of the quantitative Rietveld analysis (phase fraction, lattice parameter, and oxygen fractional parameter u) are recorded in Table I.

As can be seen in Fig. 6, the lattice parameter a of spinel Co_3O_4 exhibits a linear increase with temperature up to 950 K. Above 950 K, the lattice parameter was rapidly increased, while the oxygen fractional parameter u was sharply decreased. These results can be attributed to the cations disorder over tetrahedral and octahedral sites, which are in good agreement with a previous report [8]. In order to get more information about the cations disorder in spinel Co_3O_4 with temperature, the A-O and B-O bond lengths in the tetrahedral and octahedral sites, respectively, were calculated by Rietveld refinement (Fig. 6). Similar to lattice parameter, both A-O and B-O bond lengths show a linear increase with temperature up to 950 K, which is due to the thermal expansion of the lattice. Above 950 K, a significant decrease in the A-O bond length was observed, which can be explained by the partial substitution of smaller Co^{3+} for larger Co^{2+} cations [$r_{tetr}(Co^{3+}$, high spin) = 0.45 Å, $r_{tetr}(Co^{2+}) = 0.58$ Å; both ions are fourfold coordinated] [28]. On the other hand, the sharp increase in B-O bond length above 950 K could be attributed to the partial substitution of larger Co^{2+} for smaller Co^{3+} cations [$r_{oct}(Co^{3+}$, low spin) = 0.53 Å, $r_{oct}(Co^{2+}) = 0.72$ Å; both ions are sixfold coordinated] [28]. The cation distributions in Co_3O_4 spinel and the degree of inversion (i), which is equal to the fraction of B cations on A sites or A cations on B sites, can be calculated from bond lengths $d_{A\text{-O}}$ and $d_{B\text{-O}}$ from the relationships.

$$d_{A\text{-O}} = i r_{tetr}(Co^{3+}) + (1-i) r_{tetr}(Co^{2+}) + r_{tetr}(O^{2-}), \quad (1)$$

$$d_{B\text{-O}} = \frac{i}{2} r_{oct}(Co^{2+}) + \frac{(2-i)}{2} r_{oct}(Co^{3+}) + r_{tetr}(O^{2-}). \quad (2)$$

By using $r_{tetr}(O^{2-}) = 1.38$ Å [29], the A-O and B-O bond lengths for normal Co_3O_4 spinel (i.e., $i = 0$) are calculated to be 1.96 and 1.91 Å, respectively. Since the experimental values of A-O and B-O bond lengths are 1.935(3) and 1.9202(3) Å determined from Rietveld refinement, multiplication factors, 1.935/1.96 = 0.98778 and 1.9202/1.91 = 1.00534 for A and B sites, respectively, were introduced in the above equations to be

$$d_{A\text{-O}} = [i r_{tetr}(Co^{3+}) + (1-i) r_{tetr}(Co^{2+}) + r_{tetr}(O^{2-}] \times 0.98778, \quad (3)$$

$$d_{B\text{-O}} = \left[\frac{i}{2} r_{oct}(Co^{2+}) + \frac{(2-i)}{2} r_{oct}(Co^{3+}) + r_{tetr}(O^{2-})\right] \times 1.00534. \quad (4)$$

The increase in A-O and B-O bond lengths due to thermal expansion was determined by the linear fitting of experimental bond lengths below 950 K and extrapolating to higher-temperature data. The obtained values were subtracted from experimental values of A-O and B-O bond lengths before calculating the degree of inversion. As shown in Fig. 5, Co_3O_4 remains ordered spinel below 1000 K, and then a significant

TABLE I. Rietveld structure refinement details for slowly cooled Co_3O_4 as a function of temperature (standard deviation in parentheses).

T (K)	wt % Co_3O_4	wt % CoO	a Co_3O_4	u Co_3O_4	a CoO	R_{wp}
298	100		8.0838(1)	0.2632(3)		2.95%
623	100		8.1023(3)	0.2630(8)		2.53%
800	100		8.1158(1)	0.2632(3)		2.54%
875	100		8.1225(1)	0.2632(3)		2.56%
950	100		8.1311(1)	0.2633(4)		2.55%
1025	100		8.1438(1)	0.2622(5)		2.71%
1093	100		8.1651(2)	0.2606(5)		2.78%
1100	100		8.1672(1)	0.2601(6)		2.53%
1113	100		8.1755(3)	0.2599(8)		2.53%
1140	100		8.1884(1)	0.2593(7)		2.50%
1153	100		8.1996(2)	0.2597(4)		2.59%
1163	100		8.2031(1)	0.2574(7)		2.46%
1273		100			4.3207(1)	3.79%
300	100		8.0842(3)	0.2628(3)		2.88%

increase in the cation disordering was observed above that temperature. The highest degrees of inversion in Co_3O_4 spinel calculated from A-O and B-O bond lengths were 0.54 and 0.60, respectively, at 1163 K, which is in good agreement with previous reported values [8]. The difference between the values of degree of inversion calculated from A-O and B-O bond lengths is negligible below 1113 K and becomes remarkable at higher temperatures, which can be explained by the transition of Co^{3+} from a low-spin to a high-spin state [$r_{oct}(Co^{3+}$, high spin) = 0.61 Å] or the partial reduction of smaller Co^{3+} into larger Co^{2+} cations. In fact, thermogravimetric analysis (Fig. 3) reveals a slight weight loss in Co_3O_4 spinel heated in air above 1100 K, which suggests the releasing of oxygen from the Co_3O_4 lattice and the partial reduction of Co^{3+} into Co^{2+} as the charge compensation.

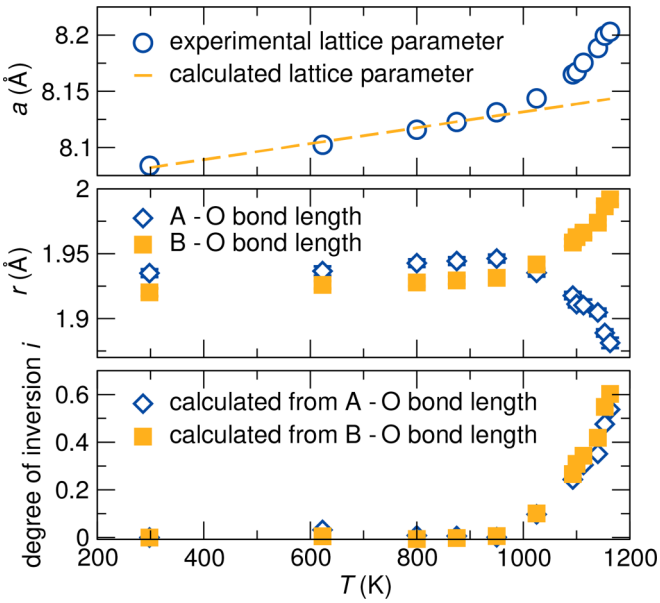

FIG. 6. Top: Lattice parameter. Middle: bond length. Bottom: degree of inversion calculated from A-O and B-O bond lengths plotted as a function of temperature.

This finding was also confirmed by XPS and redox titration analysis (Figs. 4 and 9).

Rietveld refinement was performed on neutron-diffraction data collected above and below the Néel temperature in order to determine the magnetic structure and moment (see Fig. 7). At 1.5 K, the intensity of some fundamental reflections [e.g., (111), (200), (113), (222), (331), and (420)] increased markedly but no extra reflections of magnetic origin were observed. This suggests that the magnetic unit cell is the same as the nuclear one and the magnetic structure can be

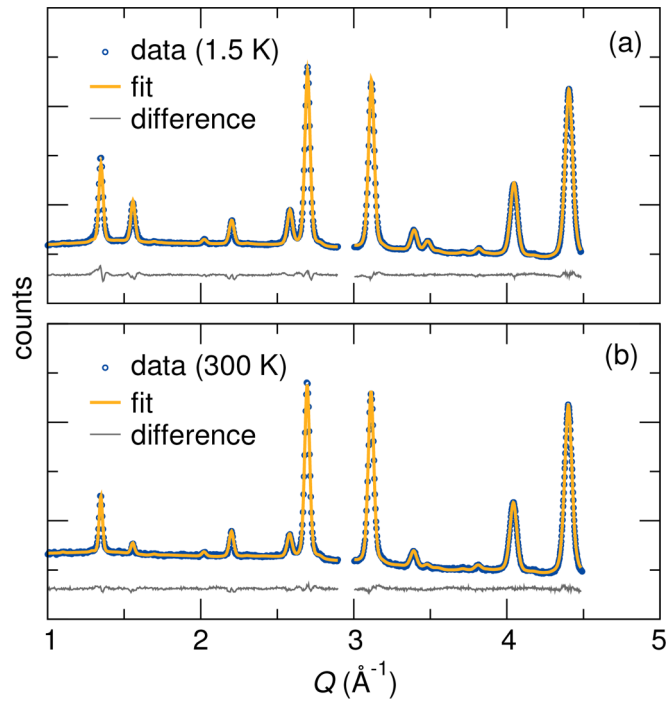

FIG. 7. Rietveld refinement was performed using neutron-diffraction patterns of a quenched Co_3O_4 sample measured (a) below (1.5 K) the Néel temperature and (b) above (300 K). The nuclear and magnetic structures are well described by the model used to determine the magnetic moment of Co^{3+}.

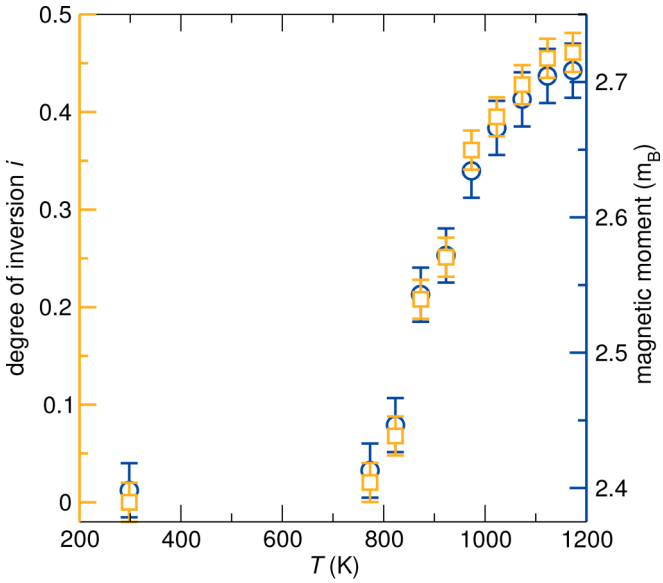

FIG. 8. The magnetic moment of Co_3O_4 (left axis) and degree of inversion calculated from the magnetic moment (right axis) increase with the quench temperature. Samples quenched from higher temperature have a greater amount of oxygen vacancies, which increases the amount of Co^{2+}.

described by a propagation vector $k = (0, 0, 0)$. The magnetic irreducible representations for the $(8a)$ and $(16d)$ sites propagation vector $k = (0, 0, 0)$ were determined using the BASIREPS program [18]. The magnetic reducible representation for the $(8a)$ site comprises two 3-dimensional irreducible representations as

$$\Gamma_{\mathrm{Co1}}^{8a} = 1\Gamma_7^{(3)} + 1\Gamma_{10}^{(3)}. \tag{5}$$

The basis vectors of $1\Gamma_7^{(3)}$ and $1\Gamma_{10}^{(3)}$ are $[(x, y, z) + (-x, -y, -z)]$ and $[(x, y, z) + (x, y, z)]$, respectively. The diffraction patterns of all samples can be well fitted with the magnetic structure corresponding to representation Γ_7 (Fig. 7). The refinements of the magnetic structure using the representation Γ_{10} for the $(8a)$ site as well as all irreducible representations determined for the $(16d)$ site yield poor fitting to the observed diffraction data. These results suggest that the magnetic structure of Co_3O_4 is due to antiferromagnetic ordering of spins in the A sites only, which is in good agreement with previous work [4]. As the quenching temperature of the samples increases, the refined magnetic moment (Fig. 8) remains roughly constant (2.4 μ_B) until 823 K, where the magnetic moment increases sharply until it reaches 2.71 μ_B in the sample quenched from 1200 K. The magnetic moment of the samples quenched from low temperature (i.e., $T < 823$ K) is in good agreement with Chen and Selloni who calculate the Co^{2+} magnetic moment to be 2.59 μ_B in bulk Co_3O_4 [5]. The increase in the magnetic moments in the A site with increasing the quenching temperature can be explained by cations disorder and the partial substitution of Co^{2+} by high-spin Co^{3+} in that tetrahedral site. On the other hand, the diffusion of Co^{2+} into the octahedral B site, which maintains the high spin state, is expected to induce a small magnetic moment in the B site. Nevertheless, no magnetic moment was observed in the B site for all samples. However, the degree of inversion in Co_3O_4 spinel can be also estimated from the overall effective magnetic moment μ_A in the A site using the equation

$$\mu_A^2 = i\mu_{\mathrm{Co^{3+}}}^2 + (1 - i)i\mu_{\mathrm{Co^{2+}}}^2, \tag{6}$$

where $\mu_{\mathrm{Co^{2+}}}$ and $\mu_{\mathrm{Co^{3+}}}$ are spin-only effective moments of Co^{2+} (3.87 μ_B) and Co^{3+} (4.89 μ_B), respectively. The theoretical effective moment in the A site for normal Co_3O_4 spinel (i.e., $i = 0$) calculated from the equation given above is 3.87 μ_B. Since the experimental effective moment value of unheated Co_3O_4 spinel, which is expected to be a normal spinel, was 2.4 μ_B, a multiplication factor, $3.87/2.4 = 1.61$, was introduced in the above equations to be

$$(\mu_A \times 1.61)^2 = i\mu_{\mathrm{Co^{3+}}}^2 + (1 - i)i\mu_{\mathrm{Co^{2+}}}^2. \tag{7}$$

As shown in Fig. 1, Co_3O_4 quenched from low temperature (i.e., $T < 823$ K) remains ordered spinel, and a significant increase in the cation disordering was observed in the samples quenched from temperatures above 823 K (see Fig. 8). The highest degree of inversion in Co_3O_4 spinel quenched from 1163 K was 0.46, which is very close to the value obtained from *in situ* XRD experiments.

XPS was performed to investigate the oxidation and spin states of the Co centers. $3d$ transition metals (TMs) in the oxide compounds exhibit the complicated nature of the electronic structure characteristic for strongly correlated systems; the shape of the photoelectron spectra is strongly influenced by the final-state effects and depends also on the TM $3d$ -O $2p$ hybridization [30]. Well-defined photoelectron peaks at the binding energies of ~780 and ~795 eV are due to spin-orbit splitting of the Co $2p$ spectrum into Co $2p_{3/2}$ and Co $2p_{1/2}$ photoemissions [Fig. 9(b)]. The spectral feature extended to higher binding energies from the main Co $2p$ photoelectron line is the charge transfer satellite. The presence of the satellite peak, S, at ~10 eV is a sign of the contribution of octahedral Co^{3+} ions with the low spin state, while the Co^{2+} ions contribute to the satellite structure at ~6 eV from the main photoelectron emission [Fig. 9(b)]. The divalent Co ions in tetrahedral coordination do not exhibit the strong intensive satellite structure [denoted as S* in Fig. 9(b)] in opposition to the octahedral Co^{2+} ions [31]. Samples quenched from lower temperatures (e.g., 300 and 773 K) have Co $2p$ spectra consistent with previous reports of Co_3O_4 [31,32].

As the quenching temperature is increased (up to 1173 K), there is no evolution in the satellite peak S corresponding to Co^{3+} ions, whereas a slight increase in the satellite peak S* corresponding to Co^{2+} was observed. Thus, *ex situ* XPS measurements suggest a small amount of octahedral Co^{2+} ions is present in the sample quenched from 1173 K [31], which confirms the results of *in situ* XRD and neutron-diffraction experiments. Another noticeable difference: Co $2p_{3/2}$ and Co $2p_{1/2}$ core-line spectra from samples quenched at high temperature (1173 K) demonstrate the main Co $2p$ photoelectron peaks with more broadening and less intensities at lower binding energies, e.g., ~779.2 and ~780.3 eV [see Fig. 9(b)]. Since the characteristic peaks of Co^{3+} ions are expected to be at binding energy lower than those of Co^{2+} ions [31,33–37], this result indicates the increase in Co^{2+} ions in the sample quenched from 1173 K in comparison with those quenched

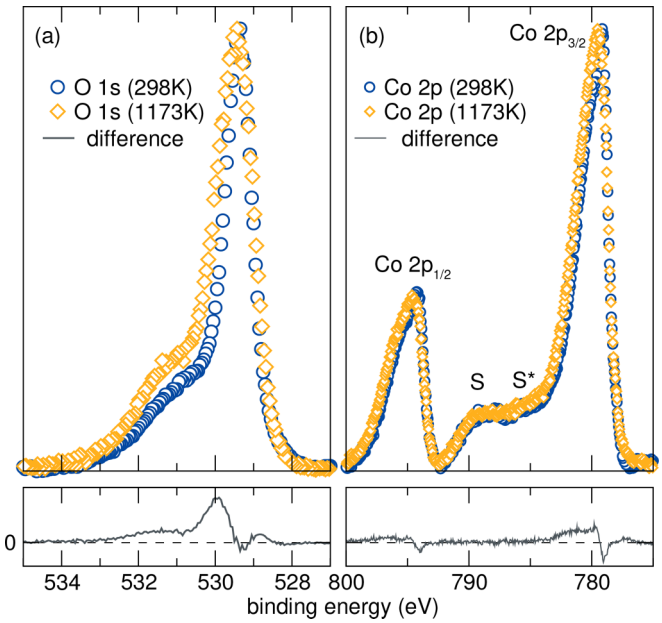

FIG. 9. (a) O 1*s* and (b) Co 2*p* photoelectron spectra of Co_3O_4 samples quenched at low and high temperatures. The spectral features S and S* are typical for Co_3O_4 with the Co^{3+} ions with LS state (satellite S) and Co^{2+} ions (satellite S*); the shape of the Co 2*p* spectra is similar for both samples. Co $2p_{3/2}$, Co $2p_{1/2}$, and O 1*s* core-line spectra from samples quenched at high temperature (1173 K) have peaks with less intensity, highlighted by the difference curve.

from lower temperature. However, the precise determination of the surface Co^{3+}/Co^{2+} ratio in samples by fitting XPS spectra is very difficult due to the controversial methods used to fit the XPS spectra of Co_3O_4 in the literature [31,33–37].

The O 1*s* spectra of both samples can be decomposed into an intense peak at ∼529.4 eV and a broader and less intense one at ∼530.8 eV, which can be assigned to lattice oxygen species and the surface adsorbed oxygen or surface oxygen defect species, respectively [31,33–37]. As shown in Fig. 9(a), the intensity of the peak at ∼530.8 eV in the spectrum of Co_3O_4 quenched from 1173 K is higher than that of the sample quenched from 300 K, which suggests the increase in the surface oxygen vacancies with increasing the quenching temperature. These results agree with the results of redox titration (Fig. 4), which shows an increase in the oxygen vacancies in Co_3O_4 spinels with increasing quenching temperatures. According to the electroneutrality principle, the larger amount of surface vacancies in the sample quenched from high temperature is due to the partial reduction of Co^{3+} into Co^{2+} at elevated temperatures.

The results of all our high-temperature characterization methods (XRD, Raman spectroscopy, thermal analysis) unambiguously show that the decomposition of Co_3O_4 to CoO occurs in air at a temperature above 1100 K. This decomposition temperature is in good agreement with the majority of previous studies including those in which the phase diagrams for the Co-O system have been calculated [22,23]. This is important because it signifies that the anomalous broadening and weakening of the Raman peaks reported here (Fig. 2), as well as those reported by others between 600 and 1000 K, must be due to changes in the Co_3O_4 spinel structure itself rather than as a result of a phase transformation to CoO.

The structural observations listed above have been attributed to two main effects: inversion of the spinel structure and spin unpairing of Co^{3+} ions on the octahedral site. Inversion of the structure implies a degree of cation mixing where both Co^{2+} and Co^{3+} ions are disordered over octahedral and tetrahedral sites. Koumoto and Yanagida suggested this leads to the rise in electrical conductivity, as electron exchange (hopping) can occur between Co^{2+} and Co^{3+} ions on either site [11]. Effectively, this is equivalent to an electron transfer from Co^{2+} to Co^{3+} (hopping): $Co_A{}^{2+}$ ($e_g{}^4t_2{}^3$, $S = 3/2$) + $Co_B{}^{3+}$ (LS, $t_{2g}{}^6\ e_g{}^0$, $S = 0$) ↔ $Co_A{}^{3+}$ (HS, $e_g{}^3t_2{}^3$, $S = 2$) + $Co_B{}^{2+}$ ($t_2g^6\ e_g{}^1$, $S = 1/2$). On the other hand, spin unpairing involves the octahedral Co^{3+} electrons going from a LS to a HS state as in $Co_B{}^{3+}$ (LS, $t_2g^6\ e_g{}^0$, $S = 0$) → $Co_B{}^{3+}$ (HS, $t_{2g}^4e_g{}^2$, $S = 2$) [38] with possible formation of an intermediate state $Co_B{}^{3+}$, with $t_{2g}^5e_g{}^1$, $S = 1$ [39].

The measurements reported in this work do not provide any additional evidence of a spin state transition in spinel Co_3O_4. However, the results of *in situ* XRD experiments and the evolution of the magnetic moment in the quenched samples does suggest inversion of the structure. It is also possible that the extinction of Raman-active modes in Co_3O_4 could be associated with inversion of the structure. While these findings suggest that *ex situ* measurements on quenched samples could potentially offer some insight into high-temperature crystal structures that are otherwise experimentally inaccessible, it is likely that the electronic transitions associated with inversion and spin state in Co_3O_4 are too rapid to be observed. Additional *in situ* measurements are needed.

IV. CONCLUSIONS

X-ray diffraction, thermal analysis, and Raman scattering of Co_3O_4 spinel are reported from room temperature up to 1273 K. Previous changes in lattice parameter and bond length were confirmed, and we report an observed extinction of Raman peaks between 600 and 1000 K. This anomaly occurs over the same temperature range as many other reported high-temperature anomalies in this compound. The phase evolution of Co_3O_4 to CoO was carefully monitored (with an observed onset in air at ∼1165 K), and does not contribute to this anomaly.

By considering the different cation sizes of Co^{3+} and Co^{2+} in octahedral and tetrahedral sites along with the changing *A*-O and *B*-O bond lengths determined by *in situ* x-ray diffraction, the degree of inversion, *i*, was calculated to reach 0.6. Samples were also quenched from high temperature for *ex situ* characterization by neutron diffraction, XPS, and chemical titration. *In situ* TGA investigation of the Co_3O_4 to CoO reaction suggests the spinel Co_3O_4 is close to the ideal oxygen stoichiometry, without large fractions of oxygen vacancies. *Ex situ* redox tirtation reveals quenching samples from above 800 K introduces a small amount of oxygen vacancies, up to ∼4% by 1100 K.

Magnetic structure refinement performed on neutron-diffraction patterns reveals the *A*-site magnetic moment increases from 2.4 μ_B to 2.7 $\mu_B$with quenching temperature, suggesting a maximum degree inversion of 0.46, in fairly

good agreement with the value based on *in situ* bond length changes. No direct evidence of spin unpairing (spin state transition from LS to HS) was observed.

ACKNOWLEDGMENTS

The authors thank Scott Speakman for his valuable help with *in situ* x-ray-diffraction experiments. The authors thank the Institut Laue-Langevin for neutron-diffraction beam time allocation (D1B). M.W.G. thanks the Leverhulme Trust for funding this research via the Leverhulme Research Centre for Functional Materials Design. A.G. thanks the Alexander von Humboldt Foundation for support through a Feodor Lynen Fellowship for Experienced Researchers, hosted by DRC at Harvard University. M.F.B. thanks the Deutscher Akademischer Austauschdienst (DAAD) for fellowship support hosted by T.D.S. at the University of Utah. T.D.S. acknowledges support from NSF CAREER Award DMR 1651668.

[1] H. Frei, Polynuclear photocatalysts in nanoporous silica for artificial photosynthesis, CHIMIA Intl. J. Chem. **63**, 721 (2009).
[2] F. Jiao and H. Frei, Nanostructured cobalt oxide clusters in mesoporous silica as efficient oxygen-evolving catalysts, Angew. Chem., Int. Ed. **48**, 1841 (2009).
[3] P. Cossee, Magnetic properties of cobalt in oxide lattices, J. Inorg. Nucl. Chem. **8**, 483 (1958).
[4] W. L. Roth, The magnetic structure of Co_3O_4, J. Phys. Chem. Solids **25**, 1 (1964).
[5] J. Chen and A. Selloni, Electronic states and magnetic structure at the Co_3O_4(110) surface: A first-principles study, Phys. Rev. B **85**, 085306 (2012).
[6] B. Touzelin, Study of the oxides of cobalt and nickel by high temperature x-ray diffraction in controlled atmosphere, Rev. Int. Hautes Temp. Refract. **15**, 33 (1978).
[7] G. M. Kale, S. S. Pandit, and K. T. Jacob, Thermodynamics of cobalt (II, III) oxide (Co_3O_4): Evidence of phase transition, Trans. Jpn. Inst. Met. **29**, 125 (1988).
[8] X. Liu and C. T. Prewitt, High-temperature X-ray diffraction study of Co_3O_4: Transition from normal to disordered spinel, Phys. Chem. Miner. **17**, 168 (1990).
[9] V. M. Brabers and A. D. D. Broemme, Low-spin–high-spin transition in the Co_3O_4 spinel, J. Magn. Magn. Mater. **104**, 405 (1992).
[10] H. S. C. O'Neill, Thermodynamics of Co_3O_4: A possible electron spin unpairing transition in Co^{3+}, Phys. Chem. Miner. **12**, 149 (1985).
[11] K. Koumoto and H. Yanagida, Electrical conduction in pure and Li substituted Co_3O_4, J. Am. Ceram. Soc. **64**, 156 (1981).
[12] K. Mocala, A. Navrotsky, and D. M. Sherman, High-temperature heat capacity of Co_3O_4 spinel: Thermally induced spin unpairing transition, Phys. Chem. Miner. **19**, 88 (1992).
[13] M. Chen, B. Hallstedt, and L. J. Gauckler, Thermodynamic assessment of the Co-O system, J. Phase Equilib. **24**, 212 (2003).
[14] T. D. Sparks, A. Gurlo, M. W. Gaultois, and D. R. Clarke, A revised model for thermopower and site inversion Co_3O_4 spinel, Phys. Rev. B **98**, 024108 (2018).
[15] B. H. Toby and R. B. Von Dreele, GSAS-II: the genesis of a modern open-source all purpose crystallography software package J. Appl. Crystallog. **46**, 544 (2013).
[16] B. H. Toby, Expgui, a graphical user interface for GSAS, J. Appl. Crystallogr. **34**, 210 (2001).
[17] J. Rodríguez-Carvajal, Recent advances in magnetic structure determination by neutron powder diffraction, Phys. B (Amste)rdam, Neth. **192**, 55 (1993).
[18] J. Rodriguez-Carvajal, BASIREPS: A program for calculating irreducible representations of space groups and basis functions for axial and polar vector properties, Solid State Phenom. **170**, 263 (2011).
[19] L. M. Khriplovich, E. V. Kholopov, and I. E. Paukov, Heat capacity and thermodynamic properties of Co_3O_4 from 5 to 307 K low-temperature transition, J. Chem. Thermodyn. **14**, 207 (1982).
[20] Y. Ikedo, J. Sugiyama, H. Nozaki, H. Itahara, J. H. Brewer, E. J. Ansaldo, G. D. Morris, D. Andreica, and A. Amato, Spatial inhomogeneity of magnetic moments in the cobalt oxide spinel Co_3O_4, Phys. Rev. B **75**, 054424 (2007).
[21] O. V. Gayduk and R. P. Pantaler, Rapid titrimetric method of cobalt (III,IV) determination by indigo carmine, Anal. Kontrol **1**, 25 (2010).
[22] I.-H. Jung, S. A. Decterov, A. D. Pelton, H.-M. Kim, and Y.-B. Kang, Thermodynamic evaluation and modeling of the Fe-Co-O system, Acta Mater. **52**, 507 (2004).
[23] A. Navrotsky, C. Ma, K. Lilova, and N. Birkner, Nanophase transition metal oxides show large thermodynamically driven shifts in oxidation-reduction equilibria, Science **330**, 199 (2010).
[24] N. Bahlawane, P. H. T. Ngamou, V. Vannier, T. Kottke, J. Heberle, and K. Kohse-Höinghaus, Tailoring the properties and the reactivity of the spinel cobalt oxide, Phys. Chem. Chem. Phys. **11**, 9224 (2009).
[25] V. G. Hadjiev, M. N. Iliev, and I. V. Vergilov, The Raman spectra of Co_3O_4, J. Phys. C **21**, L199 (1988).
[26] O. N. Shebanova and P. Lazor, Raman study of magnetite (Fe_3O_4): Laser-induced thermal effects and oxidation, J. Raman Spectrosc. **34**, 845 (2003).
[27] I. Lorite, J. Romero, and J. Fernández, Effects of the agglomeration state on the Raman properties of Co_3O_4 nanoparticles, J. Raman Spectrosc. **43**, 1443 (2012).
[28] S. Hugh, C. O'Neill, and A. Navrotsky, Simple spinels: Crystallographic parameters, cation radii, lattice energies, and cation distribution, Am. Mineral. **68**, 181 (1983).
[29] R. T. Shannon and C. T. Prewitt, Effective ionic radii in oxides and fluorides, Acta Crystallogr., Sect. B: Struct. Crystallogr. Cryst. Chem. **25**, 925 (1969).
[30] J. Zaanen, G. A. Sawatzky, and J. W. Allen, Band Gaps and Electronic Structure of transition-metal compounds, Phys. Rev. Lett. **55**, 418 (1985).
[31] S. C. Petitto, E. M. Marsh, G. A. Carson, and M. A. Langell, Cobalt oxide surface chemistry: The interaction of CoO(100),

Co_3O_4(110), and Co_3O_4(111) with oxygen and water, J. Mol. Catal. A: Chem. **281**, 49 (2008).

[32] C. A. F. Vaz, D. Prabhakaran, E. I. Altman, and V. E. Henrich, Experimental study of the interfacial cobalt oxide in $Co_3O_4/\alpha - Al_2O_3$(0001) epitaxial films, Phys. Rev. B **80**, 155457 (2009).

[33] M. C. Biesinger, B. P. Payne, A. P. Grosvenor, L. W. Lau, A. R. Gerson, and R. S. C. Smart, Resolving surface chemical states in XPS analysis of first row transition metals, oxides and hydroxides: Cr, Mn, Fe, Co, and Ni, Appl. Surf. Sci. **257**, 2717 (2011).

[34] S. Xie, H. Dai, J. Deng, Y. Liu, H. Yang, Y. Jiang, W. Tan, A. Ao, and G. Guo, Au/3DOM Co_3O_4: Highly active nanocatalysts for the oxidation of carbon monoxide and toluene, Nanoscale **5**, 11207 (2013).

[35] X. Leng, Q. Zeng, K.-H. Wu, I. R. Gentle, and D.-W. Wang, Reduction-induced surface amorphization enhances the oxygen evolution activity in Co_3O_4, RSC Adv. **5**, 27823 (2015).

[36] C. Zhang, J. Xiao, X. Lv, L. Qian, S. Yuan, S. Wang, and P. Lei, Hierarchically porous Co_3O_4/C nanowire arrays derived from a metal–organic framework for high performance supercapacitors and the oxygen evolution reaction, J. Mater. Chem. A **4**, 16516 (2016).

[37] Z. Chen, C. X. Kronawitter, and B. E. Koel, Facet-dependent activity and stability of Co_3O_4 nanocrystals towards the oxygen evolution reaction, Phys. Chem. Chem. Phys. **17**, 29387 (2015).

[38] M. Lenglet and C. K. Jørgensen, Reinvestigation of the optical properties of Co_3O_4, Chem. Phys. Lett. **229**, 616 (1994).

[39] C. N. R. Rao, M. M. Seikh, and C. Narayana, Spin-state transition in $LaCoO_3$ and related materials, in *Spin crossover in transition metal compounds II*, Topics in Current Chemistry Vol. 234, edited by P. Gütlich and H. A. Goodwin (Springer, Berlin, Heidelberg, 2004), Book section 1, pp. 1–21.